Isolated and Non-Isolated Multilevel Switching Cells with Linear Component and Stress Scaling

Matthew Jahnes
Electrical Engineering
Columbia University
New York, New York
matthew.jahnes@columbia.edu

Matthias Preindl
Electrical Engineering
Columbia University
New York, New York
matthias.preindl@columbia.edu

***Abstract*—This paper presents a framework for an adaptive power converter topology family that can be defined through software for all combination of input and output requirements. This includes buck, boost, and buck/boost operation both with and without input to output isolation. Furthermore, this framework provides methods for multilevel interpretations, allowing for it to be applied to converters of arbitrarily high voltage levels. The framework consists of a canonical switching cell upon which all converter types can be derived through selecting the corresponding input and output nodes of the cell. The canonical switching cell can be vertically stacked to achieve a multilevel interpretation of the buck, boost, and buck/boost converters. The control complexity does not increase when vertically stacked. The multilevel converter built on the proposed framework has linear component quantity, voltage stress, and current stress scaling and can be analyzed as a single canonical switching cell through a recursive approach. Topological definitions are provided alongside methods of expanding to N levels. The framework is validated through high-fidelity simulation of a multilevel iteration. This work results in a generalized concept of switching cells to N levels.**

I. Introduction

Power converters are ubiquitous in modern technology. At the small scale, personal computing devices like cellphones and laptops will contain some mixture of buck, boost, buck/boost, and/or a converter of a more exotic topology [1], [2]. Larger scale devices, like electric vehicles (EVs) [3], EV charging stations [4], or HVDC transmission systems [5], will use similar topologies in lower voltage applications or multilevel topologies for higher voltage applications.

The topology chosen for different applications is largely a product of the input and output voltage and current requirements with topological complexity as a tuneable constraint [6]–[13]. This divide in topological designs for different applications is unnecessary. This paper presents an interpretation of the dual active half bridge (DAHB) as a canonical switching cell upon which all converter input and output (buck, boost, buck/boost) characteristics can be achieved both with and without isolation. Furthermore, this canonical switching cell can be stacked in a linear manner, resulting in a multilevel interpretations of this topological framework.

Through reconfiguration and/or stacking of the canonical switching cell, buck, boost, and buck/boost of arbitrary voltage and current levels for isolated or non-isolated applications can be derived. This is a step towards dynamic power conversion, achievable through software definition and reconfiguration of a single converter or converter topology. The proposed scheme can be leveraged to take the place, or be used as a source of derivation, for any power converter for all applications.

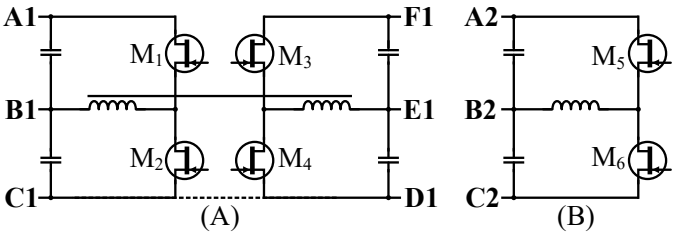

Fig. 1. Canonical switching cells. (a): Isolated canonical switching cell (DAHB), buck/boost interpretation. (b): Non-isolated canonical switching cell (half-bridge), buck interpretation.

This paper provides topological definitions of the proposed canonical switching cells as well as methods of expansion to N-levels. Applications of the canonical switching cell to different input and output requirements through reconfiguration is shown. Component quantities and voltage/current scaling as functions of N are provided. These scalings are linear. Equations for output voltage as a function of converter parameters are provided. Functionality is demonstrated through high-fidelity simulation of both isolated and non-isolated interpretations of this topological framework along with a simple switching state control scheme. This work results in a generalized concept of switching cells to N levels.

II. Individual Switching Cell Descriptions

The individual switching cell upon which this overarching topology is built on can be seen in Fig. 1-(a). This switching cell is widely known as the dual active half bridge (DAHB) and is studied extensively [14]–[16]. The DAHB of Fig. 1-(a) can be considered the isolated version of the canonical switching cell, and the circuit of Fig. 1-(b), which is topologically identical to a half-bridge converter, as the non-isolated version of the canonical switching cell.

The non-isolated canonical switching cell can be derived from its isolated counterpart. This can be seen visually as nodes A2, B2, C2 of Fig. 1-(b) align with nodes A1, B1,

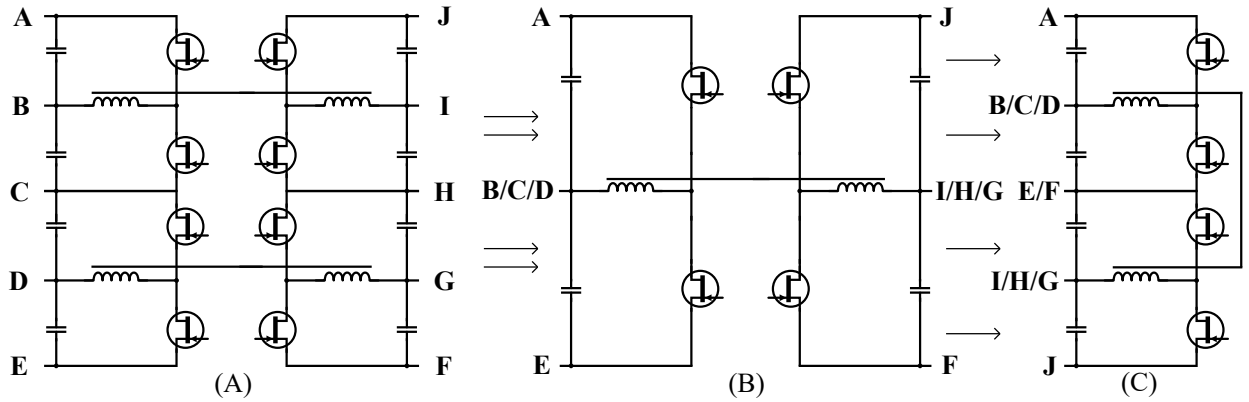

Fig. 2. Stacking of non-isolated canonical switching cells to achieve a multilevel converter. (a): Stacked multilevel isolated topology, buck/boost interpretation. (b): Canonical switching cell equivalent of (a). (c): Reconfigured iteration of (b) into a stacked non-isolated multilevel buck interpretation.

C1 of Fig. 1-(a) if there is no power transferred across the inductive coupling.

It is worth noting that Fig. 1-(a) operates and retains identical characteristics as a DAHB and Fig. 1-(b) as a half-bridge. This includes the characteristic that the ratio of capacitor voltages can be controlled to be set to any arbitrary value. Furthermore, depending on how the input and output nodes are configured, both the isolated and non-isolated canonical switching cells can act as any of the three typical power converter types (buck, boost, and buck/boost) which can be seen in Table I.

For the purpose of brevity, the polarity of nodes is not considered, the turns ratio of the isolated canonical switching cell is exclusively set to $n = 1$, and the inputs and outputs are taken from opposite sides of the coupled inductor for the isolated canonical switching cell.

Alternatively, the canonical switching cell of Fig. 1-(a) can be reconfigured into the circuit of Fig. 3-(a) through connection of nodes $C1$ and $D1$. This results in the buck/boost configuration of the isolated canonical switching cell. Identical to the previous analysis, this can be any of the three power converter types depending on which nodes are configured as input/output, as an equivalency can be drawn between the Fig. 3-(a) and Fig. 1-(b) which can be seen in Fig. 3. The circuit of Fig. 3-(a) can also be considered a multilevel topology.

TABLE I
INPUT AND OUTPUT CONFIGURATIONS OF CANONICAL SWITCHING CELLS

Converter type	Input Nodes	Output Nodes
Buck	V_{A2C2}	V_{A2B2}, V_{B2C2}
Boost	V_{A2B2}, V_{B2C2}	V_{A2C2}
Buck/boost	V_{A2B2}, V_{B2C2}	V_{B2C2}, V_{A2B2}
Buck (isolated)	V_{A1C1}	V_{F1E1}, V_{E1D1}
Buck (isolated)	V_{F1D1}	V_{A1B1}, V_{B1C1}
Boost (isolated)	V_{A1B1}, V_{B1C1}	V_{F1D1}
Boost (isolated)	V_{F1E1}, V_{E1D1}	V_{A1C1}
Buck/boost (isolated)	V_{A1B1}, V_{B1C1}	V_{F1E1}, V_{E1D1}
Buck/boost (isolated)	V_{F1E1}, V_{E1D1}	V_{A1B1}, V_{B1C1}

Furthermore, it can be expanded to an arbitrary N number of levels, which is discussed in the following section.

III. MULTILEVEL SWITCHING CELL DESCRIPTIONS

In a similar manner to the process taken to achieve Fig. 3, the canonical switching cells of Fig. 1 can be vertically stacked to achieve a multilevel topology, with input/output characteristics similar to those of the canonical switching cell. The non-isolated cell can be stacked into a multilevel converter, the results of which can be found and discussed in depth in [17].

An isolated multilevel topology can be achieved through simply stacking isolated cells. A multilevel converter of four levels can be seen in Fig. 2-(a) which consists of two stacked isolated switching cells. This isolated multilevel converter of Fig. 2 is simply two DAHBs placed on top of eachother. It can also be interpreted as as a single DAHB which can be seen in Fig. 2-(b). For a given input/output voltage and current, the sum of the power transferred over the inductive couplings of Fig. 2-(b) equal the power transferred over the inductive coupling of Fig. 2-(b). Likewise, the capacitor and switch

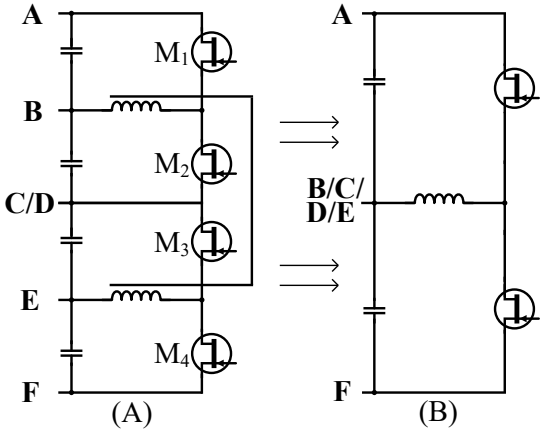

Fig. 3. (a): Reconfiguration of isolated canonical switching cell into a stacked multilevel non-isolated topology, buck interpretation. (b): Non-isolated canonical switching cell equivalent of (a), buck interpretation.

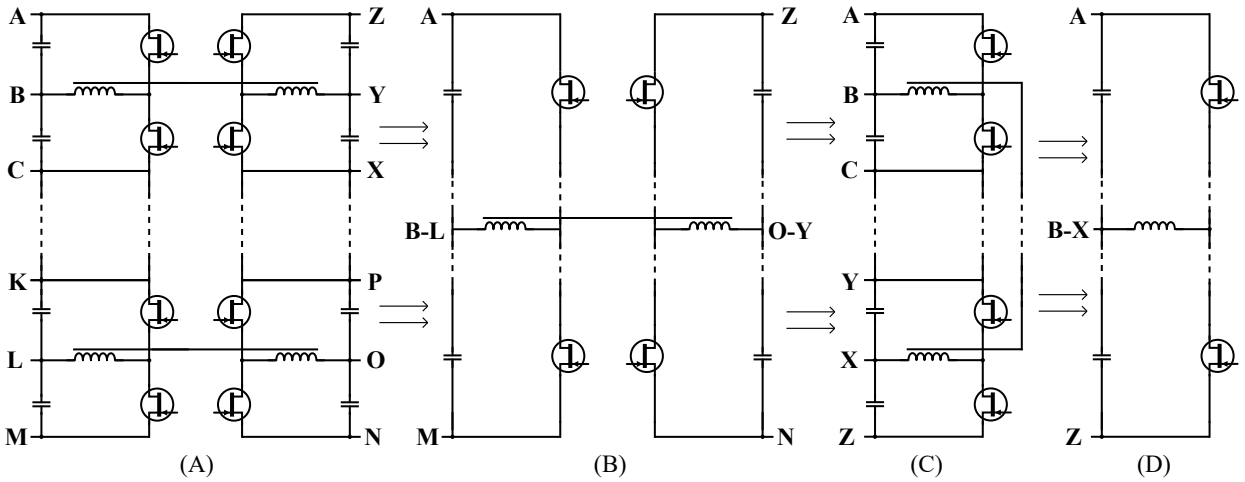

Fig. 4. Methods of expansion to N levels. a) Stacked N level isolated topology, buck/boost interpretation. b) Isolated canonical switching cell equivalent of (a). c) Reconfiguration of (a) and (b) into a multilevel buck interpretation. d) non-isolated canonical switching cell equivalent of (c).

voltage stresses of Fig. 2-(a) are split by two when compared with those of Fig. 2-(b).

Similar to the process taken in Fig. 3, the isolated multilevel circuit of Fig. 2 can be reconfigured and stacked again, resulting in Fig. 2-(c). This is a non-isolated multilevel topology, similar to that of Fig. 3, which is both composed of canonical switching cells and can be interpreted as a canonical switching cell itself. This lends this topological framework to a recursive ideology where a single canonical switching cell can be stacked and reconfigured into a larger multilevel converter, but can function in the same manner as the single canonical switching cell that it is composed of.

Furthermore, these topologies can be expanded to an arbitrary N levels. Methods of arbitrarily expanding the non-isolated canonical switching cell of Fig. 1-(b) can be found in [17]. Expanding the isolated canonical switching cell involves simply stacking additional cells on top of eachother to achieve the desired number of levels which can be seen in Fig. 4. Similar to the circuits of Fig. 2, the N-level converter of Fig. 4-(a) can also be interpreted as a canonical switching cell (Fig. 4-(b)). The isolated circuits of Fig. 4-(a,b) can then be reconfigured into a non-isolated multilevel topology of N-levels as seen in Fig. 4-(b). This non-isolated multilevel topology can also be interpreted as a non-isolated canonical switching cell (Fig. 4-(d)).

As discussed previously, each canonical switching cell can control the voltages of its capacitors to an arbitrary ratio. For the multilevel multi-cell interpretation, this allows for the entire voltage (V_{AZ} for the non-isolated topology in Fig 4-(c), V_{AM} and V_{AN} for the isolated topology in Fig. 4-(a)) to be distributed across the capacitors in any ratio, allowing for linear component stress scaling with N. As the component quantities

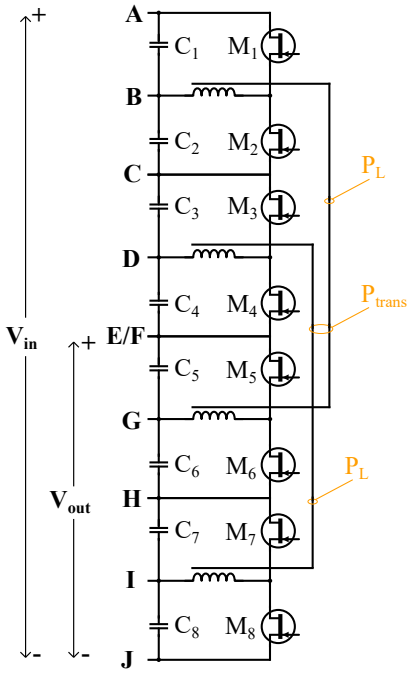

Fig. 5. Buck interpretation non-isolated multilevel converter used for results validation.

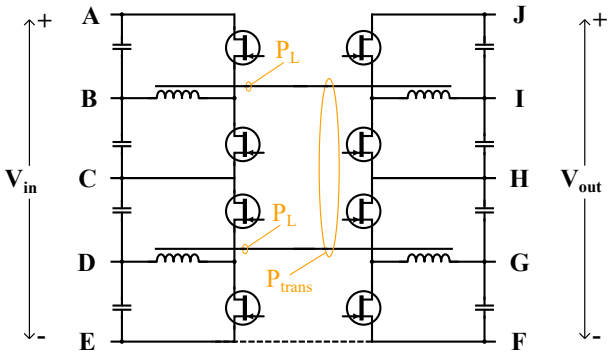

Fig. 6. Buck/boost interpretation isolated multilevel converter used for results validation.

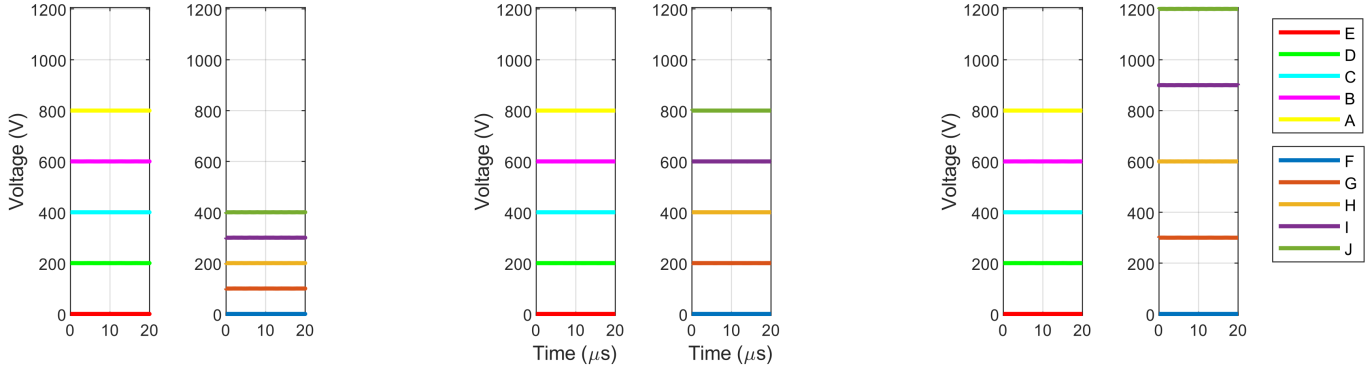

Fig. 7. Level voltages of the isolated multilevel configuration for different conversion ratios V_{out}/V_{in}. Left: conversion ratio of 0.5. Center: conversion ration of 1. Right: conversion ratio of 1.5.

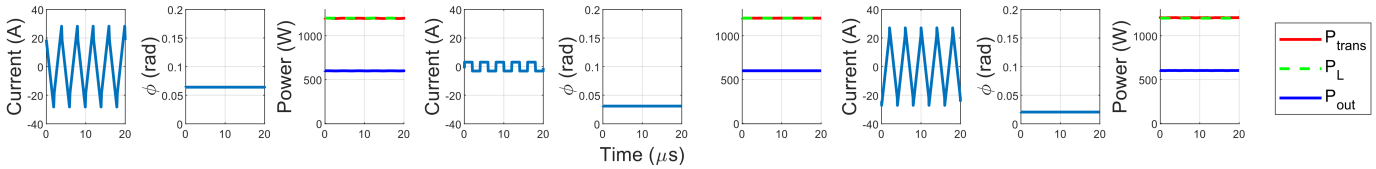

Fig. 8. Inductor current I_L, DAHB phase difference ϕ, and inductive coupling power transfer for different conversion ratios V_{out}/V_{in}. Left: conversion ratio of 0.5. Center: conversion ration of 1. Right: conversion ratio of 1.5.

also scale linearly with N, this topological framework can be considered linearly expandable with respect to both component quantities and component stresses, which is ideal for multilevel applications with very high input and output voltages.

The parameters that can be adjusted to control cell voltages and power flows are the duty cycles D of each half bridge and the total power transferred over each inductive coupling P_{trans}. For the sake of analytical simplicity, the duty cycles can all be assumed as $D = 0.5$ as this will ensure the capacitors within each half bridge have equal voltage stress. Therefore, exclusively P_{trans} can be used to adjust the operating point of the converter.

For the isolated converter, calculating the output voltage as a function of P_{trans} is straightforward as the entirety of the output power is passed through the inductive couplings. It can be seen that

$$V_{out} = \frac{P_{trans}}{I_{out}} \tag{1}$$

$$P_{trans} = \sum_{i}^{k} P_{Li}, \tag{2}$$

where k is the number of inductive couplings and P_{Li} is the power transferred over each individual inductive coupling. If the power transferred over each inductive coupling is equal, then

$$P_{Li} = P_L \tag{3}$$

$$P_{trans} = kP_L. \tag{4}$$

In this manner the output voltage V_{out} can be controlled through the sum of the power transferred over the inductive couplings. Finding the output voltage V_{out} as a function of P_{trans} for the non-isolated converter is less straightforward as only a portion of the output power needs to be transferred over the inductive coupling. The portion of the output power that needs to be transferred over the inductive coupling changes with the conversion ratio V_{out}/V_{in} of the converter and is equal to

$$\frac{P_{trans}}{P_{out}} = 1 - \frac{V_{out}}{V_{in}}. \tag{5}$$

Simple algebraic manipulation provides V_{out} as a function of P_{trans}

$$V_{out} = V_{in}\left(1 - \frac{P_{trans}}{P_{out}}\right), \tag{6}$$

where P_{trans} is the sum of power transferred across all inductive couplings. For the non-isolated topology, it is important that opposing sides of each DAHB canonical cell are on opposing sides of the output node, as power needs to be transferred from above the output node to below the output node to maintain capacitor voltage balance in steady state.

Lastly, the power transferred over a single inductive coupling P_L (for both the non-isolated and isolated) cases can be calculated with

$$P_L = \frac{V_{CL}V_{CR}}{16nL_{lk}}\phi(1-\phi), \tag{7}$$

where ϕ is the phase difference in switching cycles between opposing sides of each DAHB, normalized to the switching period. V_{CL} is the sum of capacitor voltages on one side of the DAHB and V_{CR} is the sum of capacitor voltages on the opposite side. n is the turns ratio of the coupled inductor and L_{lk} is its leakage inductance referred to one side. It is worth

noting that (7) is not unique to this topology and holds true for all DAHBs. These equations are validated in the following section.

IV. Results

The proposed toplogical framework is validated through high-fidelity simulation of the both the non-isolated circuit in Fig. 5 and the isolated circuit of Fig. 6. For the nonisolated circuit, the input voltage is applied across nodes V_{AJ} and the output taken across nodes $V_{E/F,J}$. The isolated circuit input is applied across nodes V_{AJ} and output taken across V_{JF}.

For both circuits the input voltage has a value $V_{in} = 800$V. All capacitances have the same value of 68μF. The leakage inductance of each coupled inductor is 4μH with a turns ratio of $n = 1$. The switching frequency is held contstant at $F_{sw} = 250$kHz. The duty cycle of all half-bridges is set to a constant value of $D = 0.5$. The phase difference ϕ, normalized to the switching period, is configured to be the same for all DAHBs. A single PI controller is implemented to find the required phase difference ϕ to achieve a desired output voltage V_{out}.

The output power P_{out} is held constant at 1.2kW for both circuits. A resistive load is applied that changes value over the output voltage sweep to maintain a constant output power. For the non-isolated circuit, the output voltage is swept from $0.25V_{in} \leq V_{out} \leq 0.75V_{in}$. The isolated circuit output voltage is swept from $0.5V_{in} \leq V_{out} \leq 1.5V_{in}$.

The results for the isolated circuit can be seen in Figs. 7 and 8. The input voltage is evenly split across capacitors C1-C4. The same is true for the output voltage and capacitors C5-C8. The power transferred over each inductive coupling (P_L) with the total power transferred over all inductive couplings P_{trans} equal to the output power P_{out}.

The results for the non-isolated circuit can be seen in Figs. 9, 10, 11, and 12. Capacitors C1-C4 evenly split the output voltage V_{out}. Capacitors C5-C8 evenly split the difference between the input voltage and the output voltage $V_{in} - V_{out}$. The power transferred over each inductive coupling P_L is the same for both DAHBs and the total power transferred over all inductive couplings P_{trans} is less than the output power P_{out}. This is because the power that is required to move between capacitors to maintain capacitor voltage balance is always less than the output power.

The voltage results show that the levels (and the capacitors) have ideal voltage splitting. This is beneficial for multilevel topologies, as this ensures voltage stresses across the stack of components are evenly distributed and no single switch or capacitor sees a higher voltage than necessary. This allows for control and conversion of voltages higher than the rating of any individual component.

The power results show that the output power P_{out} is effectively supported by the power transfer through the inductive couplings. For the isolated case, all output power flows through the inductive couplings. For the non-isolated case, only a proportion of the output power flows through the inductive couplings. This is because the inductive couplings do not need to support the whole output current, but only the amount of power necessary to maintain capacitor voltage balance in

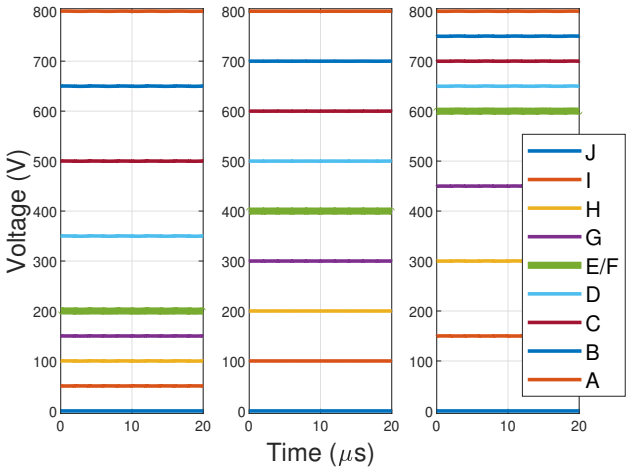

Fig. 9. Level voltages of the non-isolated multilevel configuration for different conversion ratios V_{out}/V_{in}. Left: conversion ratio of 0.25. Center: conversion ration of 0.5. Right: conversion ratio of 0.75.

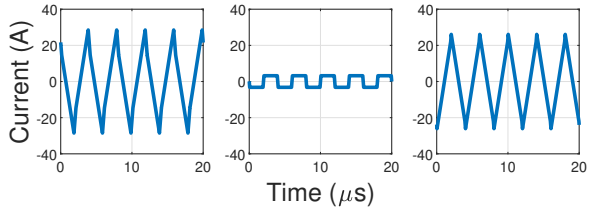

Fig. 10. Inductor currents I_L of the non-isolated multilevel configuration for different conversion ratios V_{out}/V_{in}. Left: conversion ratio of 0.25. Center: conversion ration of 0.5. Right: conversion ratio of 0.75.

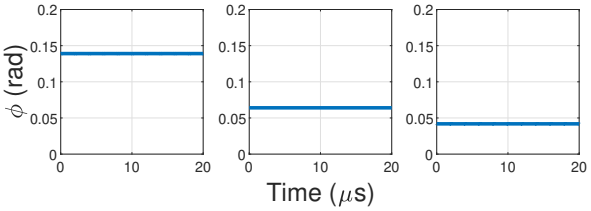

Fig. 11. DAHB phase difference ϕ of the non-isolated multilevel configuration for different conversion ratios V_{out}/V_{in}. Left: conversion ratio of 0.25. Center: conversion ration of 0.5. Right: conversion ratio of 0.75.

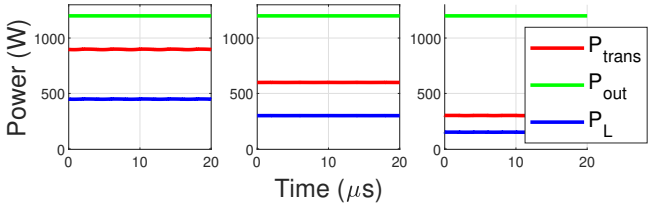

Fig. 12. inductive coupling power transfers of the non-isolated multilevel configuration for different conversion ratios V_{out}/V_{in}. Left: conversion ratio of 0.25. Center: conversion ration of 0.5. Right: conversion ratio of 0.75.

steady state. As a result, the amount of power that is converted P_{trans} is less than the output power P_{out}, an attribute unique to this converter.

Lastly, the inductor current results show that each DAHB, when configured into the proposed topological framework, still retains functional characteristics of a typical DAHB. The predicted results of (1) - (7) match the simulated results.

V. Conclusion

The topological framework developed in this paper show that the proposed canonical switching cells can be reconfigured to achieve a power converter of any arbitrary input, output, voltage, current, and isolation requirements. A single cell can be stacked vertically, without any extra topological connections and linear component quantites and stresses, to achieve a high voltage multilevel converter. Cells can also be stacked horizontally to increase current handling capabilites. Furthermore, the control complexity does not increase with the number of cells, as all steady state output voltages can be achieved by adjust a single variable (ϕ). This framework can be used to create power converters controlled through software configuration, which can allow for a single converter design to be used for any application through software reconfiguration. Further work regarding this topological framework includes physical experimental validation and investigation into optimal control methods.

References

[1] Muheng Shen. Fast simulation model of hybrid modular multilevel converters for cpu. In *2019 3rd International Conference on Electronic Information Technology and Computer Engineering (EITCE)*, pages 32–36, 2019.

[2] Li-Wei Lin, Chung-Hsing Chang, Huang-Jen Chiu, and Shann-Chyi Mou. Dual mode control multiphase dc/dc converter for cpu power. In *2006 CES/IEEE 5th International Power Electronics and Motion Control Conference*, volume 1, pages 1–5, 2006.

[3] Michael Eull, Liwei Zhou, Matthew Jahnes, and Matthias Preindl. Bidirectional nonisolated fast charger integrated in the electric vehicle traction drivetrain. *IEEE Transactions on Transportation Electrification*, 8(1):180–195, 2022.

[4] Liwei Zhou, Michael Eull, Weizhong Wang, Gangqi Cen, and Matthias Preindl. Design of transformerless electric vehicle charger with symmetric ac and dc interfaces. In *2021 IEEE Applied Power Electronics Conference and Exposition (APEC)*, pages 2769–2774, 2021.

[5] M. A. Abdel-Moamen, S. A. Shaaban, and F. Jurado. France-spain hvdc transmission system with hybrid modular multilevel converter and alternate-arm converter. In *2017 Innovations in Power and Advanced Computing Technologies (i-PACT)*, pages 1–6, 2017.

[6] A. Lavanya, J. Divya Navamani, K. Vijayakumar, and R. Rakesh. Multi-input dc-dc converter topologies-a review. In *2016 International Conference on Electrical, Electronics, and Optimization Techniques (ICEEOT)*, pages 2230–2233, 2016.

[7] E. de la Cruz, S. Ollero, J. Rodriguez, J. Uceda, and J.A. Cobos. Review of suitable topologies for on-board dc/dc converters in distributed power architectures for telecom applications. In *[Proceedings] Fourteenth International Telecommunications Energy Conference - INTELEC '92*, pages 59–65, 1992.

[8] C. Klumpner and F. Khera. Evaluation of inverter topologies for high power/medium voltage aircraft applications. In *The 10th International Conference on Power Electronics, Machines and Drives (PEMD 2020)*, volume 2020, pages 188–193, 2020.

[9] Mahajan Sagar Bhaskar, Vigna K. Ramachandaramurthy, Sanjeevikumar Padmanaban, Frede Blaabjerg, Dan M. Ionel, Massimo Mitolo, and Dhafer Almakhles. Survey of dc-dc non-isolated topologies for unidirectional power flow in fuel cell vehicles. *IEEE Access*, 8:178130–178166, 2020.

[10] Pooja Chimurkar and Pranjali Kothavade. A review of different power converter topologies for pmsgs wind turbine. In *2016 International Conference on Communication and Electronics Systems (ICCES)*, pages 1–6, 2016.

[11] Alireza Nami, Jiaqi Liang, Frans Dijkhuizen, and Georgios D. Demetriades. Modular multilevel converters for hvdc applications: Review on converter cells and functionalities. *IEEE Transactions on Power Electronics*, 30(1):18–36, 2015.

[12] Zhiqing Wang, Quanming Luo, Yuqi Wei, Di Mou, Xinlei Lu, and Pengju Sun. Topology analysis and review of three-port dc–dc converters. *IEEE Transactions on Power Electronics*, 35(11):11783–11800, 2020.

[13] Karri Hemanth Kumar and Gadi Venkata Siva Krishna Rao. A review of various dc-dc converter topologies for photovoltaic applications. In *2021 6th International Conference on Communication and Electronics Systems (ICCES)*, pages 49–52, 2021.

[14] Alberto Rodríguez Rodríguez Alonso, Javier Sebastian, Diego G. Lamar, Marta M. Hernando, and Aitor Vazquez. An overall study of a dual active bridge for bidirectional dc/dc conversion. In *2010 IEEE Energy Conversion Congress and Exposition*, pages 1129–1135, 2010.

[15] Fei Gao, Ngoni Mugwisi, and Daniel J. Rogers. Average modeling of a dual-half-bridge converter modulated with three degrees of freedom. *IEEE Transactions on Transportation Electrification*, 7(3):1016–1030, 2021.

[16] Haixu Shi, Kai Sun, Hongfei Wu, and Yunwei Li. A unified state-space modeling method for a phase-shift controlled bidirectional dual-active half-bridge converter. *IEEE Transactions on Power Electronics*, 35(3):3254–3265, 2020.

[17] Matthew Jahnes, Bernard Steyaert, and Matthias Preindl. A balanced and vertically stacked multilevel power converter topology with linear component scaling. In *IECON 2021 – 47th Annual Conference of the IEEE Industrial Electronics Society*, pages 1–6, 2021.